

Published in final edited form as:

*Anal Chem.* 2012 December 18; 84(24): 10756–10762. doi:10.1021/ac3026674.

## Acoustophoretic Sorting of Viable Mammalian Cells in a Microfluidic Device

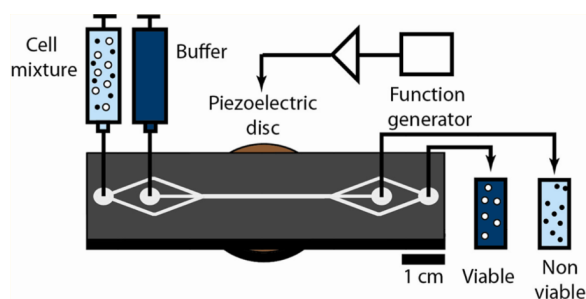
Allen H. J. Yang<sup>†</sup> and H. Tom Soh<sup>\*,†,‡,§</sup>

<sup>†</sup>Institute for Collaborative Biotechnologies, University of California, Santa Barbara, California 93106, United States

<sup>‡</sup>Department of Mechanical Engineering, University of California, Santa Barbara, California 93106, United States

<sup>§</sup>Materials Department, University of California, Santa Barbara, California 93106, United States

### Abstract



We report the first use of ultrasonic acoustophoresis for the label-free separation of viable and nonviable mammalian cells within a microfluidic device. Cells that have undergone apoptosis are physically smaller than viable cells, and our device exploits this fact to achieve efficient sorting based on the strong size dependence of acoustic radiation forces within a microchannel. As a model, we have selectively enriched viable MCF-7 breast tumor cells from heterogeneous mixtures of viable and nonviable cells. We found that this mode of separation is gentle and enables efficient, label-free isolation of viable cells from mixed samples containing  $10^6$  cells/mL at flow rates of up to 12 mL/h. We have extensively characterized the device, and we report the effects of piezoelectric voltage and sample flow rate on device performance and describe how these parameters can be tuned to optimize recovery, purity, or throughput.

There are many areas of biotechnology and medicine that would benefit from a system capable of gentle and efficient separation of viable cells from dead or nonviable cells. In monoclonal antibody production, it is necessary to remove nonviable hybridomas as these hinder the growth of neighboring viable cells and decrease overall antibody production.<sup>1</sup> The capability to separate nonviable cells is also essential in many types of cell-based therapies. For example, in hematopoietic stem cell transplantation,<sup>2</sup> the function of CD34+ stem cell grafts has been shown to be significantly reduced by the presence of apoptotic cells,<sup>3</sup> and in neurological regenerative therapy,<sup>4</sup> targeted induction of apoptosis and

\*Corresponding Author, tsoh@enr.ucsb.edu.

#### ASSOCIATED CONTENT

##### Supporting Information

Additional information as noted in the text. This material is available free of charge via the Internet at <http://pubs.acs.org>.

The authors declare no competing financial interest.

subsequent removal of malignant cells is critical for reducing tumor growth in cell grafts.<sup>5</sup> For all of these applications, the ideal separation method would be label-free, sufficiently gentle to preserve cellular health and function, and capable of high-throughput operation. Unfortunately, conventional separation methods such as centrifugation, fluorescence-activated cell sorting (FACS), and magnetic-activated cell sorting (MACS) do not meet all of these requirements.<sup>6</sup>

Microfluidic technology offers a compelling alternative, because it allows precise control over separation forces coupled with the potential to considerably increase throughput by operating multiple microchannels in parallel.<sup>7</sup> Since the seminal work of Markx and co-workers,<sup>8</sup> several reports have described the use of dielectrophoresis (DEP) for the label-free separation of viable from nonviable cells based on their different electrical properties.<sup>9–12</sup> Unfortunately, the use of DEP has proven challenging because dielectrophoretic forces are highly sensitive to buffer conditions (e.g., salt concentration) and only allow relatively low sample throughput (typically <100 cells/s per microchannel).<sup>6</sup> Beyond DEP, there are few examples of microfluidic devices that utilize alternative forces for the label-free separation of viable cells.

In this work, we have investigated the use of ultrasonic standing waves within microchannels<sup>13,14</sup> toward the separation of viable mammalian cells from a mixture containing apoptotic cells of the same type. This approach offers many advantages, because acoustophoretic forces are relatively insensitive to pH, salt concentration, and other media properties, potentially allowing a wider range of sample matrices and enabling their use in cell separation applications. Importantly, the acoustic radiation force strongly depends on cell volume, which enables us to successfully discriminate smaller apoptotic cells from larger viable cells of the same type. To effectively utilize this force in a microchannel, we adopted a device architecture pioneered by Johnson and Feke<sup>15</sup> and used by many other groups, including ours.<sup>16–21</sup> Our chip employs a multistream lateral flow architecture and uses a piezoelectric disk to create a resonant standing acoustic wave within the main separation channel (Figure 1). As cells pass through the acoustic field, a size-dependent radiation pressure force preferentially focuses larger, viable cells toward the center line of the channel for collection. This radiation pressure force acts orthogonally to the direction of flow and therefore places minimal stress on the cells. We show that our chip can handle sample throughputs of up to 12 mL/h at a density of  $10^6$  cells/mL, which is significantly higher than previously demonstrated with DEP.<sup>11</sup> Finally, we characterize the device's performance as a function of piezoelectric actuation voltage and sample flow rate, and we quantify the effect of these parameters on recovery and purity.

## EXPERIMENTAL SECTION

### Device Fabrication

Standard photolithography and etching procedures were used to fabricate the acoustophoretic device microchannels. Hexamethyldisiloxane (Sigma–Aldrich) was spun onto a clean 100 mm diameter, 500  $\mu\text{m}$  thick silicon wafer at 4000 rpm for 30 s for priming, after which a 1.4  $\mu\text{m}$  layer of AZ5214E-IR photoresist (Clariant, Somerville, NJ) was spun at 3000 rpm and baked at 95  $^{\circ}\text{C}$  for 2 min. The microchannels were patterned using broadband photolithography followed by a 2 min image-reversal bake at 115  $^{\circ}\text{C}$  and 1 min flood exposure. The microchannels were etched to a depth of 56  $\mu\text{m}$  via a Bosch deep reactive-ion etching process using the photoresist layer as an etch mask. After removal of the photoresist with acetone, inlet and outlet holes were manually drilled using a CNC drill press (Flashcut CNC, Deerfield, IL) with a 0.75 mm diameter diamond bit (Triple Ripple, Abrasive Technology, Lewis Center, OH). A fused silica wafer was anodically bonded to the silicon wafer by applying a 1000 V bias at 375  $^{\circ}\text{C}$  for 5 min. The wafer was diced into

individual devices, and brass inlet/outlet eyelets and the 2 cm diameter piezoelectric transducer (PZ26, Ferroperm, Kvistgaard, Denmark) were attached using 5 min epoxy (Devcon, Danvers, MA) and permanent glue (Henkel Consumer Adhesives, Avon, OH) respectively.

### Cell Preparation Protocol

MCF-7 cells were revitalized from liquid nitrogen storage and suspended in 1 mL of culture media containing Eagle's minimum essential medium (EMEM) supplemented with 10% fetal bovine serum (FBS) and 1% penicillin/streptomycin. All culture reagents were purchased from ATCC (Manassas, VA). Cells were then incubated in T-150 cell culture flasks (Fisher Scientific) with 30 mL of culture media until they reached 90% confluence. The cells were washed with Dulbecco's phosphate-buffered saline (DPBS; ATCC), released using 5 mL of trypsin/EDTA solution (ATCC), and then collected and pelleted via centrifugation at 400g for 10 min. Live cells were resuspended in 10 mL of PBS/BSA (PBS and 2% BSA). Nonviable cells were prepared by taking a fraction of the total cell suspension (according to the intended final viable/nonviable ratio) and pelleting the cells via centrifugation, followed by resuspension in 10 mL of 10× PBS and incubation at room temperature for 30 min. Apoptotic MCF-7 cells were washed and resuspended in PBS/BSA with the live cells to a final cell concentration of  $10^6$  cells/mL.

### Acoustic Cell Separation

The microfluidic device was preloaded with a solution of filtered deionized water and degassed to remove bubbles in the tubing. Cell samples and suspension buffer were pumped into the device through their respective inlets via syringe pump (Harvard Apparatus, Holliston, MA) at a 1:3 ratio of sample/buffer flow rate. We aliquoted 1 mL of the cell sample from the syringe to determine the initial viable/nonviable cell composition. The piezoelectric disk was actuated with a sinusoidal signal from a function generator (33120A, Hewlett-Packard, Palo Alto, CA) that had been passed through a linear amplifier (LT1210, Linear Technologies, Milpitas, CA) that swept from 2.02 to 2.06 MHz at a sweep rate of 1 ms. We observed separation at the outlet junction using an inverted microscope (TE2000-S, Nikon, Melville, NY) fitted with a 10× objective and connected to a CCD camera (CoolSNAP HQ2, Photometrics, Tuscon, AZ) for imaging. The device outlets were connected by elastic tubing (Tygon tubing, o.d. 0.09 in., i.d. 0.05 in.; Saint-Gobain Performance Plastics, Aurora, OH) to 2 mL centrifuge tubes for collection. After operation, we cleaned the device with a solution of 20% bleach and rinsed with filtered, deionized water.

### Cell Staining and Flow Cytometry Analysis

We collected 1 mL aliquots of the acoustically separated cell populations from each outlet of the device. For cell characterization, in combination with flow cytometry, we used a fluorescent staining kit (LIVE/DEAD viability/cytotoxicity kit, Life Technologies, Carlsbad, CA) to label viable and nonviable cell populations. Each vial of cells was treated with 1  $\mu$ L of calcein/DMSO (green viable cell stain) and 1  $\mu$ L of ethidium homodimer-1 (red nonviable cell stain), each prepared from stock solutions provided in the staining kit, and then subjected to agitated incubation on a rotating holder for 20 min in the dark at room temperature. We used an Accuri C6 flow cytometer (BD Biosciences, San Jose, CA) to analyze 20  $\mu$ L samples from each vial, measuring forward-scattering, side-scattering, and fluorescence using the FL1 and FL3 filters. To measure the diameters of our cells, we imaged them under 20× magnification in a Olympus BX60 microscope (Center Valley, PA) with a differential image contrast filter and then analyzed the images using the ImageJ software package with a known pixel-length calibration. A large number of cells (>1000) were sampled from the device eluent to ensure that we had accurately determined cell

recovery and purity. We normalized cell counts to account for flow-rate differences between the device outlets during flow cytometry. Recovery ( $R$ ) was calculated as the number of viable cells in the collection outlet divided by the sum of viable cells in both the collection and waste outlets. Contamination ( $C$ ) was calculated similar to recovery but using nonviable cell counts. Purity ( $P$ ) was calculated as the number of viable cells in the collection outlet divided by the total number of cells eluted via the collection outlet.

## RESULTS AND DISCUSSION

### Device Design and Fabrication

The chip measures 60 mm  $\times$  20 mm  $\times$  1 mm ( $L \times W \times T$ ) and is fabricated from a silicon substrate etched with microchannels, which is anodically bonded to a fused silica substrate. The details of the fabrication process are shown in the Supporting Information, Figure 1. There are two inlets (sample/buffer) and two outlets (collection/waste), and the sample is divided into two streams that sandwich the buffer stream within the separation channel. The device is acoustically driven by an external piezoelectric actuator attached to the silicon substrate of the device. Recent articles have discussed design considerations in building standing wave acoustofluidic devices,<sup>22,23</sup> such as acoustic streaming effects<sup>24</sup> and temperature effects from joule heating.<sup>25,26</sup> Our separation channel within the device is 3 cm  $\times$  350  $\mu\text{m}$   $\times$  50  $\mu\text{m}$  ( $L \times W \times T$ ) and will support a standing acoustic half-wave with a pressure node at the channel center at a resonant frequency of 2.04 MHz. Cells passing through the separation region will experience an acoustic radiation force described by the following equation:<sup>27,28</sup>

$$F_{ac} = 4\pi a^3 k_0 E_0 \left[ \frac{\rho_c + \frac{2}{3}(\rho_c - \rho_m)}{2\rho_c + \rho_m} - \frac{1}{3} \frac{\kappa_c}{\kappa_m} \right] \sin(2k_0 z) \quad (1)$$

where  $a$  is the cell radius,  $k_0$  is the angular wavenumber,  $E_0$  is the acoustic energy density,  $z$  is the position coordinate aligned with the width of the device,  $\rho$  is the density, and  $\kappa$  is the compressibility, with subscripts c and m representing the cell and suspension medium, respectively. Thus, the difference in acoustophoretic force ( $F_{ac}$ ) exerted on a viable cell compared to a nonviable cell is determined by differences in their density, compressibility, and volume.

The separation mechanism is based on differences in  $F_{ac}$ , which result in different steady-state velocities ( $U_{ac}$ ) for viable and nonviable cells toward the center line of the device. This velocity can be defined as follows:

$$U_{ac} = \frac{F_{ac}}{6\pi a \eta} \quad (2)$$

where  $\eta$  is the fluid viscosity. Based on eqs 1 and 2, if we consider a mixture of viable and nonviable cells that differ in density, compressibility, and volume, we can express the ratio of the time needed for viable and nonviable cells to focus at the center line as the following:

$$\frac{\tau_v}{\tau_{nv}} = \frac{U_{nv}}{U_v} \quad (3)$$

where  $\tau$  is the focusing time and subscripts v and nv refer to viable and nonviable cells, respectively. However, if we approximate the viable and nonviable cells as having the same density and compressibility, as confirmed by previously reported measurements of MCF-7 acoustic properties before and after apoptosis,<sup>29</sup> then eq 3 reduces to the following:

$$\frac{\tau_v}{\tau_{nv}} = \left( \frac{V_{nv}}{V_v} \right)^{2/3} \quad (4)$$

where  $V$  is the cell volume. Given enough time, all cells will reach the separation channel center, but optimal separation of viable and nonviable cells is attained when the cell residence time, or the time that cells spend within the main separation channel, lies between  $\tau_v$  and  $\tau_{nv}$ . To achieve this condition, we tuned two experimental parameters: piezoelectric voltage, which affects  $E_0$  and governs  $\tau_v$  and  $\tau_{nv}$ , and sample flow rate, which controls cell residence time.

### Model Cell System and Viability Assay

Necrosis and apoptosis are cell death pathways that can be triggered by changes in the cellular environment. Necrosis, or traumatic cell death, involves the swelling and bursting of mammalian cells, while apoptosis, or natural cell death, results in cell shrinkage, changes in membrane permeability, and collapse of the nucleus and cytoskeleton.<sup>30</sup> We distinguished viable from nonviable cells within our cell mixtures using a two-color fluorescent viability assay and flow cytometry. For our experiments, we used MCF-7 human breast cancer cells, a cell line widely used in cancer research.<sup>31</sup> MCF-7 cells are adherent, and we used trypsin/EDTA to suspend them in solution (see the Experimental Section). In general, this method has been reported to cause cell death in less than 10% of mammalian cells.<sup>32</sup> We observed two distinct populations when we generated forward- versus side-scatter plots after performing flow cytometry with a population of MCF-7 cells harvested using trypsin/EDTA detachment, wherein nonviable cells (5.6%) clustered to the left of viable cells (93.1%) in the forward-scatter axis as a result of cell shrinkage during apoptosis<sup>33</sup> (Figure 2A, left). This shrinkage is a general phenomenon that occurs with all mammalian cells and is a key indicator of apoptosis in these cells.<sup>34</sup> To better differentiate and quantify these two populations, we utilized a two-color viability assay in which we incubated the cells with two fluorescent stains. Ethidium homodimer-1 exclusively penetrates the membranes of nonviable cells and stains the chromosomal DNA, emitting strong red fluorescence (emission = 635 nm), whereas the calcein AM dye emits green fluorescence (emission = 515 nm) only after being converted to calcein by intracellular esterases and binding to calcium ions within the cytoplasm of live cells. Consistent with the scattering measurements above, viable cells exhibited high green fluorescence and low red fluorescence (92.3%), and nonviable cells exhibited high red fluorescence and low green fluorescence (4.4%) (Figure 2A, right).

We generated mixed populations containing predetermined ratios of viable and nonviable cells by spiking a controlled number of apoptotic cells into a population of viable cells. To induce apoptosis, we exerted osmotic stress on the cells by incubating them in high-salinity buffer (10× PBS) for 30 min. This method is well established to trigger death in both mammalian and plant cells.<sup>35,36</sup> These apoptotic MCF-7 cells underwent the same physical shrinkage as naturally occurring nonviable cells, and cells analyzed from a 60/40 mixture of viable and nonviable cells fell within the previously defined gates (Figure 2B, left). A study conducted by Strohm et al.<sup>29</sup> observed similar cell shrinkage but minimal changes in acoustic properties between viable and apoptotic MCF-7 cells. We measured the size of our viable and nonviable MCF-7 cells using microscopy and observed diameters of  $18.4 \pm 2.1$   $\mu\text{m}$  and  $15.5 \pm 1.9$   $\mu\text{m}$  for viable and nonviable cell populations, respectively. After subjecting these cells to the two-color viability assay, we observed appropriate fluorescence profiles for both viable and nonviable cell populations, with nonviable cells representing 38% of the total population (Figure 2B, right).

## Device Operation and Cell Viability

We first identified suitable operating ranges of piezoelectric voltage and sample flow rate to separate viable and nonviable MCF-7 cells in the device. To do so, we prepared a  $10^6$  cells/mL suspension of MCF-7 cells in PBS with 2% BSA, or PBS/BSA, containing a 40/60 mixture of viable/nonviable cells. Flow cytometry analysis of the initial sample confirmed that 40.3% of the cells were viable and 59.7% were nonviable (Figure 3A, top). We operated the device at a piezo-actuation voltage of 14 V, pumped cell suspension and buffer into the device at flow rates of 5 and 15 mL/h, respectively, and subsequently performed flow cytometry on the eluent from both the collection and waste outlets of the device. As discussed in the Experimental Section, we use three parameters, recovery ( $R$ ), contamination ( $C$ ), and purity ( $P$ ), to quantify the separation performance in our chip.

We confirmed that acoustic actuation leads to preferential focusing of viable cells toward the collection outlet, resulting in efficient sorting of viable and nonviable cells. Under the above operating conditions, we observed significant enrichment of viable cells ( $R = 0.94$ ) at the collection outlet with relatively low levels of nonviable cells ( $C = 0.12$ ), yielding a population for which  $P = 0.91$  (Figure 3A, middle). In the absence of piezoactuation, we observed that  $R = 0.05$  and  $C = 0.014$ , indicating that the majority of both viable and nonviable cells remained in their initial streamlines and were subsequently eluted via the waste outlet (Figure 3A, bottom). We observed a small amount of false-positive separation in the absence of piezo-actuation; however, the clear preferential enrichment of viable cells over nonviable cells with piezo-actuation demonstrates that acoustic focusing is the dominant factor in separating the two populations of cells.

Acoustic separation within our chip does not appear to affect the viability of the processed cells. To determine this, we collected cells from both outlets, washed them with PBS/BSA, incubated them in growth media, and observed their proliferation over time. As a positive control, we seeded subcultured MCF-7 cells in a culture flask at the same concentration as the chip-processed cells, determined for each sample using a hemacytometer. After five days, we observed considerable proliferation in both the positive control and chip-processed cells cultured from the collection outlet, whereas cells cultured from the waste outlet showed no apparent growth (Figure 3B). This demonstrates that the sorting process effectively isolated the viable cell population.

## Effect of Piezo-Actuation Voltage on Separation Performance

The piezoelectric actuation voltage has a considerable impact on separation performance because it directly governs the acoustic energy density ( $E_0$ ) as described in eq 1. To measure this effect, we performed a sweep of actuation voltages ranging from 4–17 V peak-to-peak for samples containing a 50/50 mixture of viable and nonviable MCF-7 cells (Figure 4A). As we increased the actuation voltage, we observed greater recovery of viable cells caused by the exertion of stronger acoustophoretic forces on cells passing through the separation channel. Contamination is minimal at low actuation voltages, as cell shrinkage suppresses acoustophoretic focusing of nonviable cells; however, contamination starts to increase significantly above 14 V.

Interestingly, we also found that  $P$ , but not  $R$  and  $C$ , is strongly dependent upon the ratio of viable to nonviable cells in the initial sample. Starting from samples containing different viable/nonviable cell ratios, we processed the cells at different actuation voltages (4–17 V) and a constant flow rate of 5 mL/h and measured the effects on  $P$  (Figure 4B). We observed that, for all mixtures tested,  $P$  was highest at voltages between 12 and 14 V. For example, samples containing a small fraction (0.1) of viable cells could be enriched at 12 V to  $P = 0.81$ , a >800% increase in purity. Actuation voltages outside this range resulted in less

reproducible separation, as indicated by larger error bars in Figure 4B. Importantly, the difference between optimal  $P$  and  $P$  obtained at the lowest and highest voltages was significantly greater for the 10/90 and 25/75 viable/nonviable cell mixtures compared to 50/50 and 75/25 mixtures. Although  $P$  varied greatly at different cell mixing ratios, we observed that there were minimal differences in  $R$  and  $C$  between the different ratios (Supporting Information, Figure 2).

Separating viable cells with high  $P$  requires conditions that yield both high  $R$  and low  $C$ . For a 50/50 mixture of cells,  $P$  was greatest at 14 V, where viable cell recovery was high ( $R = 0.81$ ) with minimal contamination from nonviable cells ( $C = 0.11$ ) (Figure 4A). We observed decreased  $P$  at voltages other than 14 V:  $R$  is lower below 14 V, whereas  $C$  increases significantly above 14 V. For example, at 6 V, there was very little contamination ( $C = 0.03$ ), but we also observed poor recovery of viable cells ( $R = 0.10$ ), resulting in low output purity ( $P = 0.49$ ). On the other hand, operation at 17 V resulted in highly efficient recovery of viable cells ( $R = 0.98$ ) but at the cost of high levels of contamination ( $C = 0.34$ ), leading to low purity ( $P = 0.57$ ). These two phenomena have a more pronounced effect in samples with low viable/nonviable ratios (Figure 4B). Compared to mixtures with higher ratios, the loss of equivalent numbers of cells in mixtures with lower ratios translates to a larger fraction of the overall population. By the same token, operation at high voltages with low-ratio mixtures results in significantly higher contamination than with high-ratio mixtures, because of the larger initial numbers of nonviable cells.

### Effect of Flow Rate on Separation Performance

Increasing sample flow rate increases the throughput of the chip but at the cost of decreased recovery of viable cells. This occurs because increased flow rates lead to shorter cell residency within the device and therefore decrease the available time for acoustic focusing. Accordingly, it is essential to identify operating conditions that optimize both throughput and recovery. To do so, we measured  $R$  and  $C$  at sample flow rates ranging from 4 to 12 mL/h at a constant actuation voltage of 17 V with a sample containing a 50/50 mix of viable and nonviable MCF-7 cells (Figure 5A). We observed a monotonic decrease in  $R$  at increasing flow rates; at the lowest flow rate (4 mL/h), we achieved  $R = 0.91$ , and the highest flow rate tested (12 mL/h) resulted in  $R = 0.30$ . Increasing the sample throughput 3-fold therefore yielded a 3-fold reduction in the recovery of viable cells, resulting in a net zero gain in the number of viable cells obtained postseparation. On the other hand, contamination was nearly 10-fold lower at 12 mL/h ( $C = 0.03$ ) compared to 4 mL/h ( $C = 0.22$ ) (Figure 5B). Accordingly, we observed a notable improvement in  $P$  from 0.60 at 4 mL/h to 0.79 at 8 mL/h.

Interestingly, however, we did not observe any further improvement in  $P$  at higher flow rates. We suspect that this apparent purity limit is partly due to the natural polydispersity in the size of both viable and nonviable cells, and Figure 2B (left) reveals some overlap in their size distributions. Another consideration is the variability in the initial spatial position of cells across the channel (i.e., orthogonal to the direction of flow) due to stream broadening near the inlet. This occurred more often when we operated the chip at higher flow rates, resulting in cells occupying positions near the wall of the channel or near the interface between the sample and buffer streams. This variability in each cell's starting position affects the time needed to focus cells to the center stream ( $\tau_v$  and  $\tau_{nv}$ ), resulting in both false-positive (higher  $C$ ) and false-negative (lower  $R$ ) separations that ultimately lead to lower  $P$ . However, even with these limitations, De Boer et al.<sup>3</sup> showed that an ideal, fresh stem-cell graft would need to contain ~90% viable cells to be most effective, and we are able to achieve similar purity at most cell mixing ratios using our device. We believe enhancements to the microfluidic architecture such as those employed by Mao et al. and others,<sup>37,38</sup> wherein the initial position of the cells is tightly controlled, could improve cell

discrimination in our device. In addition, it would be interesting to consider a multistage device architecture that could simultaneously improve both recovery and purity.<sup>20,39</sup>

## CONCLUSION

We report the first use of ultrasonic standing waves in microchannels to selectively and efficiently purify viable cells from mixtures of healthy and apoptotic cells. The underlying device physics exploit the fact that cells that have undergone apoptosis are smaller than viable cells, and we utilize the strong volume dependence of acoustic radiation forces and residence time of the cells within our microdevice to separate the two populations. Using a proliferation assay, we show that our acoustic separation technique does not affect the viability of the cells. Using flow cytometry to measure our separation performance, we systematically explored two key operating parameters (i.e., piezo-actuation voltage and flow rate) and measured their effect on purity, recovery, and throughput to optimize the separation process. Given that cell-based therapies are showing promise in treating a variety of diseases,<sup>40</sup> devices capable of gentle, label-free separation of viable cells at high recovery, purity, and throughput could prove valuable in many areas of biomedicine.

## Supplementary Material

Refer to Web version on PubMed Central for supplementary material.

## Acknowledgments

The authors would like to acknowledge Dr. Wen Hsieh and Dr. Scott Ferguson for technical discussions. Financial support for this work was generously provided by the ARO Institute for Collaborative Biotechnologies (W911NF-09-D-0001 and W911NF-10-2-0114), NIH Midwestern Progenitor Consortium, and the Otis Williams Fellowship from the Santa Barbara Foundation. Fabrication of the devices was carried out at the UCSB Nanofabrication facility.

## REFERENCES

1. Gregory CD, Pound JD, Devitt A, Wilson-Jones M, Ray P, Murray RJ. *mAbs*. 2009; 1:370. [PubMed: 20068393]
2. Passier R, van Laake LW, Mummery CL. *Nature*. 2008; 453:322. [PubMed: 18480813]
3. De Boer F, Drager AM, Pinedo HM, Kessler FL, Monnee-Van Muijen M, Weijers G, Westra G, Van der Wall E, Netelenbos T, Oberink JW, Huijgens PC, Schuurhuis GJ. *J. Hematother. Stem Cell Res*. 2002; 11:951. [PubMed: 12590710]
4. Li JY, Christophersen NS, Hall V, Soulet D, Brundin P. *Trends Neurosci*. 2008; 31:146. [PubMed: 18255164]
5. Bieberich E, Silva J, Wang GH, Krishnamurthy K, Condie BG. *J. Cell. Biol.* 2004; 167:723. [PubMed: 15545317]
6. Gossett DR, Weaver WM, Mach AJ, Hur SC, Tse HTK, Lee W, Amini H, Di Carlo D. *Anal. Bioanal. Chem.* 2010; 397:3249. [PubMed: 20419490]
7. Adams JD, Soh HT. *JALA*. 2009; 14:331. [PubMed: 20161387]
8. Marx GH, Talary MS, Pethig RJ. *Biotechnol.* 1994; 32:29.
9. Lapizco-Encinas BH, Simmons BA, Cummings EB, Fintschenko Y. *Anal. Chem.* 2004; 76:1571. [PubMed: 15018553]
10. Li HB, Bashir R. *Sens. Actuators, B*. 2002; 86:215.
11. Shafiee H, Sano MB, Henslee EA, Caldwell JL, Davalos RV. *Lab Chip*. 2010; 10:438. [PubMed: 20126683]
12. Lewpiriyawong N, Kandaswamy K, Yang C, Ivanov V, Stocker R. *Anal. Chem.* 2011; 83:9579. [PubMed: 22035423]

13. Harris NR, Hill M, Beeby S, Shen Y, White NM, Hawkes JJ, Coakley WT. *Sens. Actuator, B.* 2003; 95:425.
14. Hawkes JJ, Coakley WT. *Sens. Actuator, B.* 2001; 75:213.
15. Johnson DA, Feke DL. *Sep. Technol.* 1995; 5:251.
16. Petersson F, Aberg L, Sward-Nilsson AM, Laurell T. *Anal. Chem.* 2007; 79:5117. [PubMed: 17569501]
17. Petersson F, Nilsson A, Holm C, Jonsson H, Laurell T. *Lab Chip.* 2005; 5:20. [PubMed: 15616735]
18. Grenvall C, Augustsson P, Folkenberg JR, Laurell T. *Anal. Chem.* 2009; 81:6195. [PubMed: 19572705]
19. Lenshof A, Ahmad-Tajudin A, Jaras K, Sward-Nilsson AM, Aberg L, Marko-Varga G, Malm J, Lilja H, Laurell T. *Anal. Chem.* 2009; 81:6030. [PubMed: 19594154]
20. Adams JD, Soh HT. *Appl. Phys. Lett.* 2010:97.
21. Thevoz P, Adams JD, Shea H, Bruus H, Soh HT. *Anal. Chem.* 2010; 82:3094. [PubMed: 20199060]
22. Bruus H. *Lab Chip.* 2012; 12:1578. [PubMed: 22430330]
23. Dual J, Schwarz T. *Lab Chip.* 2012; 12:244. [PubMed: 22109106]
24. Barnkob R, Iranmanesh I, Wiklund M, Bruus H. *Lab Chip.* 2012; 12:2337. [PubMed: 22522812]
25. Adams JD, Ebbesen CL, Barnkob R, Yang AHJ, Soh HT, Bruus HJ. *Micromech. Microeng.* 2012:22.
26. Augustsson P, Barnkob R, Wereley ST, Bruus H, Laurell T. *Lab Chip.* 2011; 11:4152. [PubMed: 21989571]
27. Nilsson A, Petersson F, Jonsson H, Laurell T. *Lab Chip.* 2004; 4:131. [PubMed: 15052353]
28. Yosioka K, Kawasima Y. *Acustica.* 1955; 5:167.
29. Strohm, EM.; Pasternak, M.; Mercado, M.; Rui, M.; Kolios, MC.; Czarnota, GJ. A comparison of cellular ultrasonic properties during apoptosis and mitosis using acoustic microscopy. *Proceedings of the IEEE Ultrasonics Symposium; October 11–14; San Diego, CA, USA. Institute of Electrical and Electronics Engineers; 2010. p. 608*
30. Alberts, B.; Wilson, JH.; Hunt, T. *Molecular Biology of the Cell.* 5th ed. New York: Garland Science; 2008.
31. Levenson AS, Jordan VC. *Cancer Res.* 1997; 57:3071. [PubMed: 9242427]
32. Corver WE, Cornelisse CJ, Hermans J, Fleuren GJ. *Cytometry.* 1995; 19:267. [PubMed: 7736872]
33. Ormerod MG, Paul F, Cheetham M, Sun XM. *Cytometry.* 1995; 21:300. [PubMed: 8582253]
34. Elmore, S. *Toxicol. Pathol.* 2007; 35:495.
35. Affenzeller MJ, Darehshouri A, Andosch A, Lutz C, Lutz-Meindl U. *J. Exp. Bot.* 2009; 60:939. [PubMed: 19213813]
36. Michea L, Ferguson DR, Peters EM, Andrews PM, Kirby MR, Burg MB. *Am. J. Physiol. Renal.* 2000; 278:F209.
37. Hur SC, Tse HTK, Di Carlo D. *Lab Chip.* 2010; 10:274. [PubMed: 20090998]
38. Mao XL, Lin SCS, Dong C, Huang TJ. *Lab Chip.* 2009; 9:1583. [PubMed: 19458866]
39. Bessette PH, Hu XY, Soh HT, Daugherty PS. *Anal. Chem.* 2007; 79:2174. [PubMed: 17253874]
40. Jenq RR, van den Brink MRM. *Nat. Rev. Cancer.* 2010; 10:213. [PubMed: 20168320]

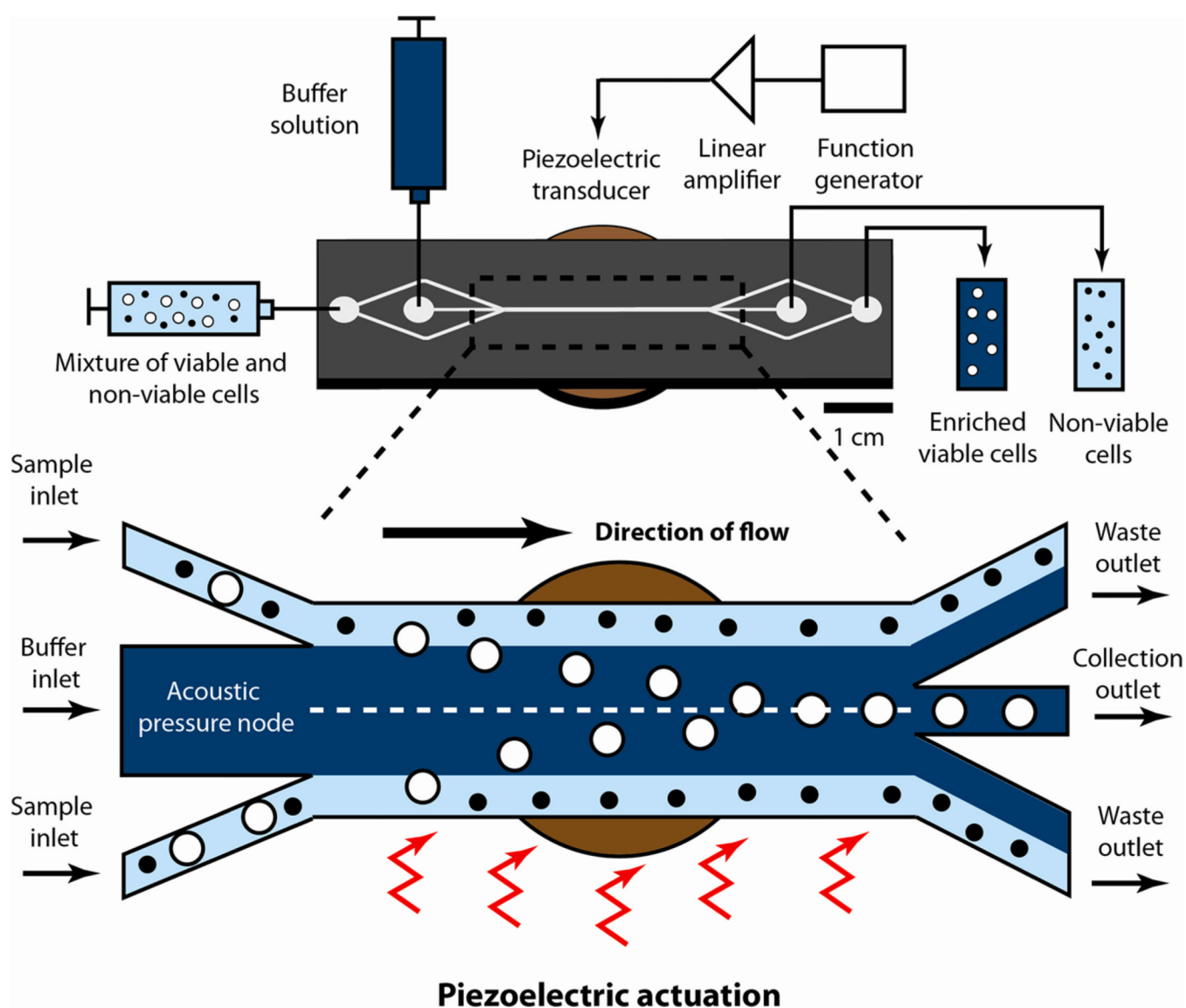


**Figure 1.** Microacoustic viability separation. The chip uses acoustophoresis to achieve label-free, high-throughput separation of viable and nonviable mammalian cells. A mixture (light blue) of viable (white) and nonviable (black) mammalian cells and a stream of suspension buffer (dark blue) are injected into the device via separate inlets at a 1:3 flow-rate ratio. The resulting colaminar flow keeps the cells close to the walls of the separation channel. Piezoelectric actuation generates an acoustic radiation force that preferentially focuses larger, viable cells toward the acoustic pressure node within the center streamline, enabling these cells to exit via the collection outlet. This force is insufficient to focus the smaller, nonviable cells to the center streamline, and they exit the device via the waste outlet.

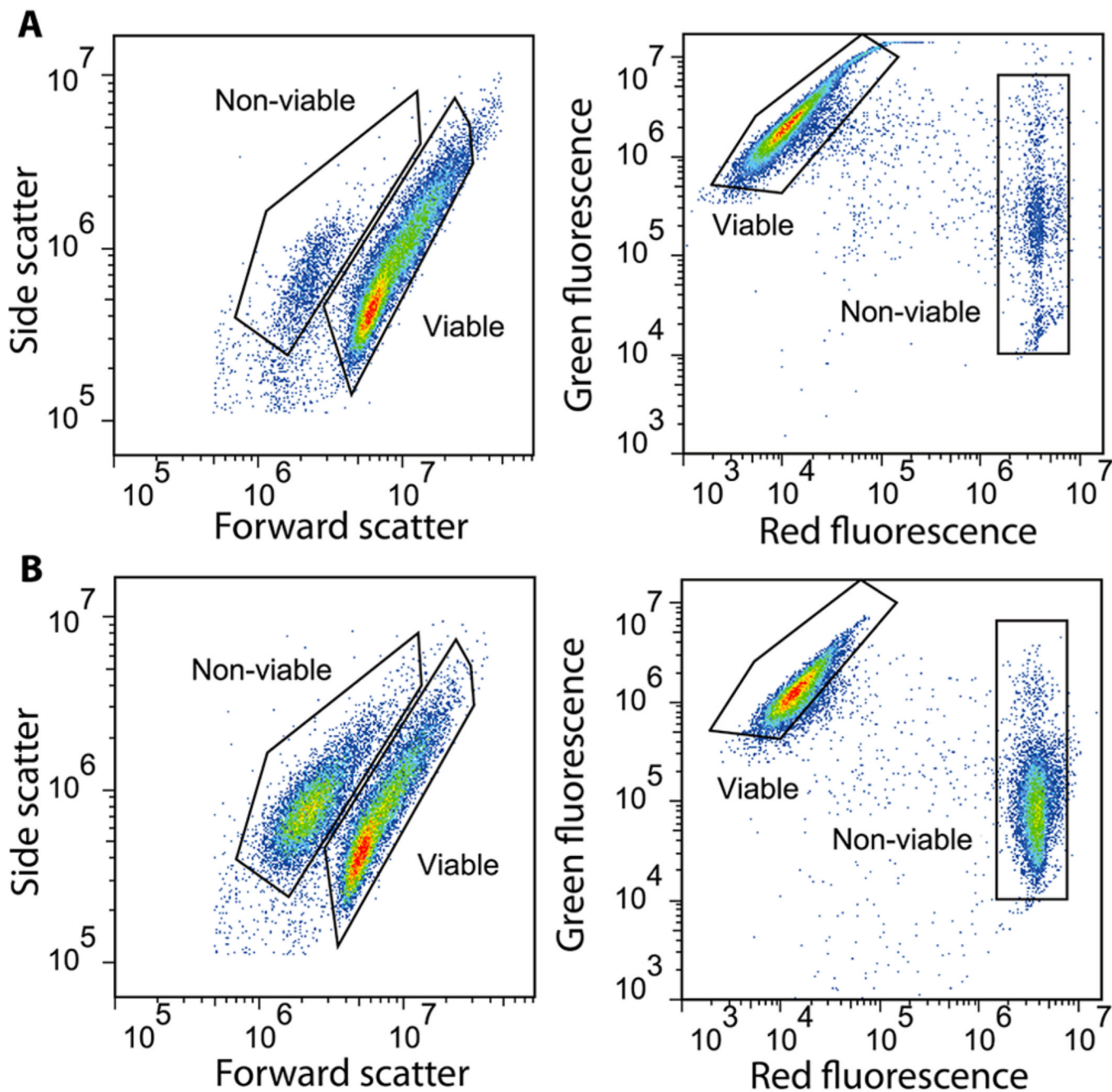


**Figure 2.** Generating defined mixtures of viable/nonviable cells. Flow cytometry analysis of mixtures of viable and nonviable MCF-7 cells. Left plots show forward- and side-scattering intensities, and right plots show cells subjected to a two-color fluorescence assay that labels viable cells green and nonviable cells red. (A) In untreated cell solutions, the vast majority of cells (92.3–93.1%) are viable. (B) We subsequently tested our ability to generate defined mixtures of viable/nonviable cells by using high-salt PBS to induce apoptosis and analyzed a 60:40 mixture of viable/nonviable cells using the same cytometric gates. Our results confirmed that the resulting mixtures reflect the intended ratios.

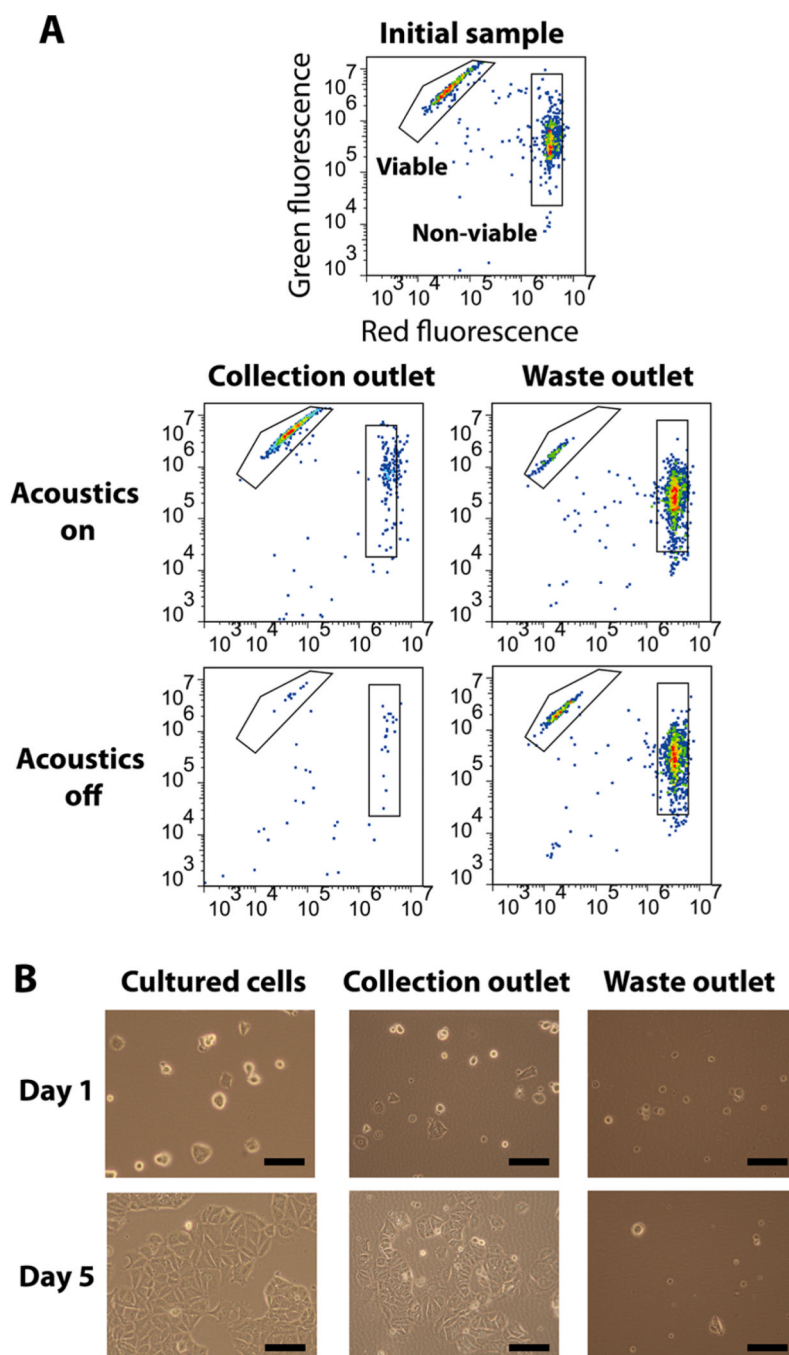


**Figure 3.** Microchannel acoustophoresis achieves effective separation without damaging cells. (A) We used the same two-color fluorescence described above with flow cytometry to identify the proportion of viable and nonviable cells in the starting population prior to separation (top) and in samples collected after performing separation with (middle) or without (bottom) acoustic actuation. Gates are drawn to identify the viable and nonviable cell populations and are consistent across all plots. (B) Microscopic images of cells cultured after passing through the device at the highest voltage (17 V) used in our study. Control cells cultured from the stock solution (left) and collection outlet (middle) proliferated extensively after

five days. In contrast, cells cultured from the waste outlet (right) showed only minimal growth. Scale bars = 100  $\mu\text{m}$ .

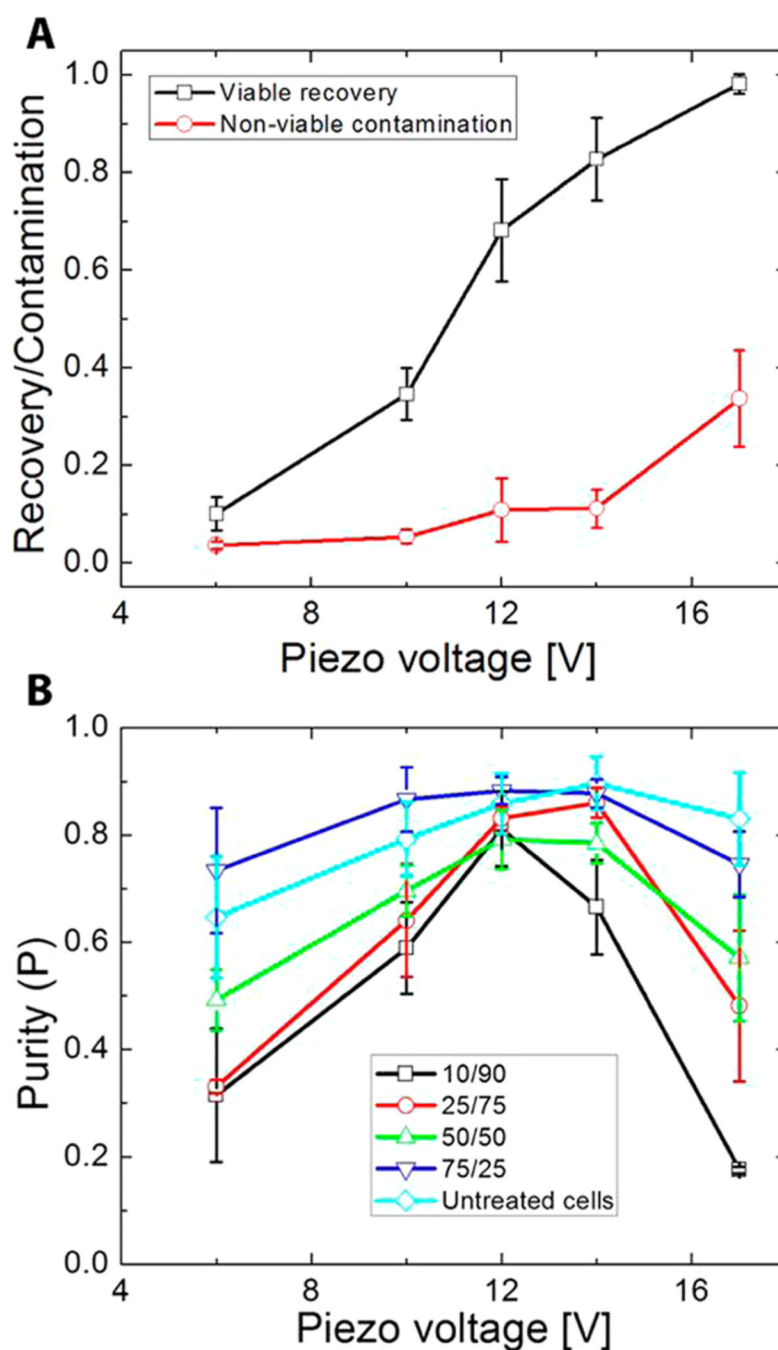


**Figure 4.** Effect of actuation voltage on device performance. (A) Plot of MCF-7 cell recovery and nonviable cell contamination as a function of actuation voltage at a constant sample flow rate of 5 mL/h from an initial 50/50 mixture of viable and nonviable cells. The red and black traces indicate contamination of nonviable and recovery of viable cells, respectively. (B) Plot of purity ( $P$ ) as a function of actuation voltage at a constant sample flow rate of 5 mL/h. As shown in the legend, each line represents a different starting ratio of viable/nonviable cells. Data from untreated MCF-7 cells is included for comparison. Error bars in both plots represent the standard deviation obtained from triplicate experiments.

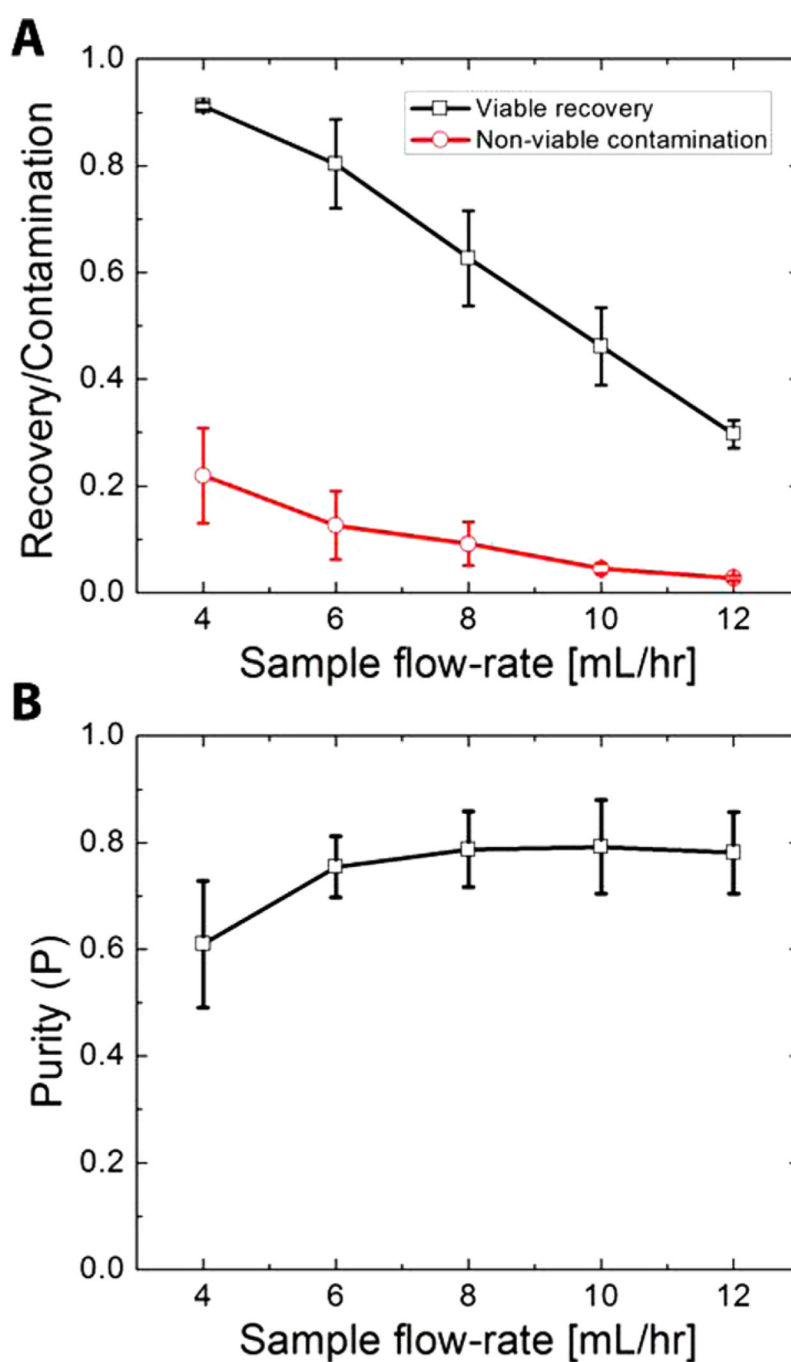


**Figure 5.** Effect of flow rate on device performance. (A) Plot of viable cell recovery and nonviable contamination as a function of sample flow rate at a constant piezo voltage of 17 V. (B) Plot of purity as a function of sample flow rate at a constant piezo voltage of 17 V. Both plots were obtained from separation of a 50:50 suspension of viable and nonviable MCF-7 cells. Error bars in both plots represent the standard deviation obtained from triplicate experiments.